Journal of Solid State Chemistry 182 (2009) 2924–2929

Contents lists available at ScienceDirect

Journal of Solid State Chemistry

journal homepage: www.elsevier.com/locate/jssc

Investigation of substitution effects and the phase transition in type-I clathrates $Rb_xCs_{8-x}Sn_{44}\square_2$ ($1.3 \le x \le 2.1$) using single-crystal X-ray diffraction, Raman spectroscopy, heat capacity and electrical resistivity measurements

Andreas Kaltzoglou [a], Thomas F. Fässler [a,*], Christian Gold [b], Ernst-Wilhelm Scheidt [b], Wolfgang Scherer [b], Tetsuji Kume [c], Hiroyasu Shimizu [c]

[a] Technische Universität München, Department Chemie, Lichtenbergstraße 4, D-85747 Garching, Germany
[b] University Augsburg, Institute of Physics, Germany
[c] Department of Materials Science and Technology, Gifu University, Japan

ARTICLE INFO

Article history:
Received 31 March 2009
Received in revised form
14 July 2009
Accepted 18 July 2009
Available online 25 July 2009

Keywords:
Alkali metals
Cation substitution
Electrical conductivity
Heat capacity
Raman spectroscopy
Type-I clathrates

ABSTRACT

The substitution of cations in $Rb_xCs_{8-x}Sn_{44}\square_2$ ($1.3 \le x \le 2.1$) is reported. The compounds crystallize at room temperature in the space group $Ia\bar{3}d$ adopting the type-I clathrate $2 \times 2 \times 2$ superstructure with partly ordered framework vacancies ($\square$), whereas at higher temperatures they transform to the primitive, more disordered modification (space group $Pm\bar{3}n$). The guest atom distributions in the Sn cages on the Rb: Cs ratios is studied by means of single-crystal X-ray diffraction for $Rb_{2.1(1)}Cs_{5.8(1)}Sn_{44}$ at $T = 293$ K (**1**), $Rb_{1.42(8)}Cs_{6.58(8)}Sn_{44}$ at $T = 293$ K (**2a**), $Rb_{1.46(5)}Cs_{6.54(5)}Sn_{44}$ at $T = 373$ K (**2b**) and $Rb_{1.32(8)}Cs_{6.68(8)}Sn_{44}$ at $T = 293$ K (**3**). The structural order–disorder phase transition influences the electrical resistivity. The hysteresis observed for the electrical resistivity in combination with the symmetric shape of the specific heat anomaly suggests that the transformation is of first-order type and is characterized by an entropy change of about 2.5 J mol^{-1} K^{-1}. The Raman spectrum for the low-temperature modification of **2** is also reported.

1. Introduction

Type-I clathrates represent a fascinating class of inclusion compounds in which two kinds of interconnected polyhedra—tetrakaidecahedra (*tkad*) and pentagonal dodecahedra (*pdod*) (Fig. 1)—form a network of tetravalent atoms. It is well established that the binary Sn homologues that encapsulate alkali metals (A) can only exist as $A_8Sn_{44}\square_2$ [1,2]. Due to the eight excess electrons from the alkali metals and the relatively low Sn–Sn bonding energy, two vacancies per cell are energetically favored over the occupation of conduction band states. Thus as expected for an electron-precise Zintl phase the compounds are semiconductors [3]. The distribution of the host vacancies in $A_8Sn_{44}\square_2$ (A = Rb, Cs) has been recently reinvestigated. In contrast to the earlier reports a partial ordering of the vacancies occurs under formation of $2 \times 2 \times 2$ superstructure (space group $Ia\bar{3}d$) [4]. An enantiotropic order–disorder phase transition from the α form ($Ia\bar{3}d$) to the high-temperature β form ($Pm\bar{3}n$) with lower ordering of the vacancies occurs at 353 K and at 363 K for Rb_8Sn_{44} and Cs_8Sn_{44}, respectively [5,6].

It was found that the phase transition affects significantly the electrical transport properties of Rb_8Sn_{44}, as the more disordered modification exhibits higher electrical conductivity and Seebeck coefficient (in absolute value) [6]. However, the spark plasma sintering of the clathrate into a pellet caused partial decomposition to β-Sn which exhibits metallic properties. In the present study we emphasize on the role of the alkali metals in $Rb_xCs_{8-x}Sn_{44}O_2$, namely their exact distribution in the cavities, by X-ray diffraction studies as well as their influence on the vibrational modes by Raman spectroscopy. Moreover, the effect of the phase transition on the heat capacity and electrical resistivity is investigated for $Rb_{1.42}Cs_{6.58}Sn_{44}$.

2. Experimental

The clathrates Rb_8Sn_{44}, $Rb_{2.1(1)}Cs_{5.8(1)}Sn_{44}$ (**1**), $Rb_{1.42(8)}Cs_{6.58(8)}Sn_{44}$ (**2**), and $Rb_{1.32(8)}Cs_{6.68(8)}Sn_{44}$ (**3**) were prepared by fusion of the pure elements, which were handled in an Ar-filled glove box (O_2- and H_2O-level <0.1 ppm). Amounts of Rb (ampoule, 99.6%, Aldrich), Cs (ampoule, >98%, Riedel de Haën) and Sn (granules, 99.999%, Chempur) in molar ratios Rb:Cs:Sn = 8:0:44, 6:2:44 and 2:6:44 (total mass 1–1.5 g) were loaded into Nb ampoules and sealed under reduced Ar pressure. The ampoules were subsequently enclosed in evacuated silica tubes, heated to 973 K for 12 h

* Corresponding author. Fax: +49 89 289 13186.
E-mail address: Thomas.Faessler@lrz.tum.de (T.F. Fässler).

0022-4596/$ - see front matter © 2009 Elsevier Inc. All rights reserved.
doi:10.1016/j.jssc.2009.07.034

(+2 K min^{-1}), cooled (−1 K min^{-1}) to 723 K, held at this temperature for 5 days and then cooled to ambient temperature.

The resulting products were identified on a Stoe STADI P powder diffractometer equipped with a Linear Position Sensitive Detector, using Cu$K\alpha$ radiation ($\lambda = 1.5406$ Å, $10^\circ \leq 2\theta \leq 90^\circ$, step width $= 0.01^\circ$). The patterns were indexed by the software package WinXPOW (Stoe) and refined with the WinPLOTR program [7].

Good quality single-crystals were obtained by annealing the samples at 723 K. Single-crystals of **3** were obtained after annealing of **2** at 723 K for 40 days. Diffraction data sets were collected at room temperature on an Oxford Xcalibur3 CCD diffractometer with graphite monochromated Mo$K\alpha$ radiation ($\lambda = 0.71073$ Å) for **1**, **2a**, and **3**. The reflections were collected over the range $2\theta_{max} = 50.6^\circ$ and corrected for absorption (multi scan) using the program CrysAlis RED (Oxford Diffraction Ltd). For structure solution and refinement (direct methods, full matrix least-square on F^2, anisotropic atomic displacement parameters for all atoms, empirical absorption corrections) SHELX97 by Bruker was used [8]. In all refinements, the sum of the site occupation factors (SOFs) for mixed occupied positions was constrained to unity (Table 1). Multi-temperature diffraction experiments were carried out on an APEX II diffractometer equipped with a rotating anode (Nonius, FR591) and an open-flow N_2 blower (Oxford cryostream cooler 700). Full data collections were performed for a crystal of **2** at 293 K (**2a**), 373 K (**2b**), and then again at 293 K heating rate (± 2 K min^{-1}). The room-temperature refinements were of comparable quality to the one collected using the Oxford Xcalibur3 diffractometer. Since data sets of crystals of **1** and **3** were also collected using the Oxford Xcalibur3 diffractometer those data are given in Table 1. Further details of the crystal structure investigations are available from the Fachinformationszentrum Karlsruhe, D-76344 Eggenstein-Leopoldshafen (Germany) on quoting the depository numbers CSD-420475 (**1**), CSD-420476 (**2a**, at 293 K), CSD-420477 (**2b**, at 373 K) and CSD-420477 (**3**), the name of the authors and citation of the paper.

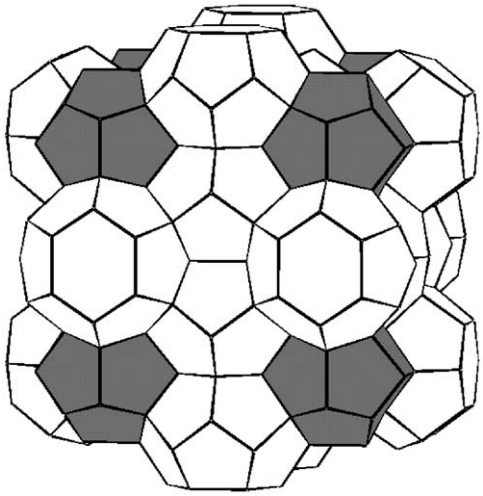

Fig. 1. Structure of the type-I clathrate with pentagonal dodecahedra (*pdod*, gray) and tetrakaidecahedra (*tkad*, white) at the ratio 1:3.

In contrast to Ref. [6] the temperature-dependent resistivity ($\rho(T)$) measurements of **2** and Rb_8Sn_{44} were performed on single-crystals employing a physical property measurement system (PPMS) of quantum design and a standard four-probe dc method with a constant dc current of 0.1 mA. The $\rho(T)$ data were collected in the temperature range 250–400 K during the respective cooling and heating sequences in a rate of 0.7 K min^{-1}. Taking the uncertainty in the determination of the non-uniform sample shape into account an absolute error bar of 30% should be assumed for the residual resistivity of **2**.

The temperature-dependent heat capacity ($C(T)$) was investigated by means of a quasi-adiabatic step heating technique as implemented in the PPMS. The measurements were performed using a powdered sample of **2a** (ca. 12 mg), which was pressed into a pellet at 1.4 GPa. The pellet was thermally connected with the specific heat measuring device via Apiezon-N and Apiezon-H grease at temperatures ranging from 1.8 K up to 300 K and from

Table 1
Crystallographic data and refinement parameters for the **1**–**3**.

Empirical formula	$Rb_{2.1(1)}Cs_{5.9(1)}Sn_{44}$ **(1)**	$Rb_{1.42(8)}Cs_{6.58(8)}Sn_{44}$ **(2a)**	$Rb_{1.46(5)}Cs_{6.54(5)}Sn_{44}$ **(2b)**	$Rb_{1.32(8)}Cs_{6.68(8)}Sn_{44}$ **(3)**
Formula (weight/g mol^{-1})	6183.79	6218.22	6216.38	6223.20
Temperature (K)	293	293	373	293
Diffractometer	Oxford Xcalibur3	Oxford Xcalibur3	APEX II	Oxford Xcalibur3
Wavelength (Å)	0.71073	0.71073	0.71073	0.71073
Space group	$Ia\bar{3}d$	$Ia\bar{3}d$	$Pm\bar{3}n$	$Ia\bar{3}d$
Z	8	8	1	8
Unit cell parameter (a/Å)	24.1764(1)	24.197(1)	12.0878(2)	24.2015(2)
Unit cell volume (V/Å^3)	14131.1(1)	14167(1)	1766.21(5)	14175.1(2)
$\rho_{calcd.}$ (g cm^{-3})	5.815	5.831	5.844	5.832
Absorption coeff. (μ/mm^{-1})	19.661	19.488	19.547	19.459
F (000)	20815	20915	2614	20930
θ range (deg)	3.15–25.31	3.77–25.32	2.38–30.50	3.15–25.28
No. of integrated reflections	43741	42009	5605	41731
No. of independent reflections	1082 ($R_{int} = 0.054$)	1085 ($R_{int} = 0.076$)	508 ($R_{int} = 0.031$)	1080 ($R_{int} = 0.072$)
No. of parameters	55	55	24	55
Goodness-of-fit on F^2	1.136	1.021	1.127	1.116
Weighting parameters[a]	$a = 0.0223$	$a = 0.0525$	$a = 0.0125$	$a = 0.0263$
	$b = 1089.1$	$b = 0$	$b = 2.623$	$b = 425.4$
Final R indices[a]	$R_1 = 0.037$	$R_1 = 0.032$	$R_1 = 0.019$	$R_1 = 0.030$
	$wR_2 = 0.078$	$wR_2 = 0.087$	$wR_2 = 0.035$	$wR_2 = 0.071$
Final R indices (all data)	$R_1 = 0.049$	$R_1 = 0.046$	$R_1 = 0.032$	$R_1 = 0.043$
	$wR_2 = 0.086$	$wR_2 = 0.091$	$wR_2 = 0.037$	$wR_2 = 0.077$
Residual map (e Å^{-3})	+0.97, −0.91	+1.04, −1.07	+0.64, −0.57	+0.74, −0.97

[a] $w = 1/[\sigma^2(F_o^2) + (aP)^2 + bP]$ where $P = (F_o^2 + 2F_c^2)/3$.

300 K up to 400 K, respectively. The uncertainty of the data points reported here is estimated to be below 5%.

Raman measurements were carried out with an apparatus, which has been improved through detecting the low-frequency signals for various clathrate compounds [9–11]. Radiation of 532 nm from a solid-state laser (Verdi2W) was incident on the sample with a power of 5 mW. The backscattered Raman spectrum was measured with a spectrometer (JASCO NR1800) equipped with a triple polychromator and a charge coupled device detector. The illuminated spot was $< 5\,\mu m$ in size and the resolution of the spectra was about $1\,cm^{-1}$.

3. Results and discussion

Different reaction stoichiometries were investigated in order to obtain a view of the substitution trends. More specifically, the products $Rb_{2.12}Cs_{5.88}Sn_{44}$ (**1**) and $Rb_{1.42}Cs_{6.58}Sn_{44}$ (**2a**) were obtained from the loading mixtures Rb:Cs:Sn = 6:2:44 and 2:6:44, respectively. Annealing of the reaction product from the latter stoichiometry for 40 days at 723 K gave rise to $Rb_{1.32}Cs_{6.68}Sn_{44}$ (**3**).

The powder patterns of **1**–**3** were indexed as superstructures of the type-I clathrate (see also supporting information) [5]. The compositions of the clathrates were refined with higher accuracy from the single-crystal data (Table 2) and depend only slightly on the reaction stoichiometry. In all cases, the amount of Sn was fixed to 44 Sn atoms per unit cell for the final structural refinement. Also the mixed occupancy for Rb and Cs is observed in the cationic sites 16*a* and 48*g* (Fig. 2) for all compounds. Cs atoms occupy preferably the centers of *tkad* rather than the *pdod* (Fig. 3). The **2** and **3** differ only in the occupation factors of the alkali metals in the *pdod*. As indicated by the anisotropic displacement parameters in Table 3, the loosely-bound alkali metals "rattle"

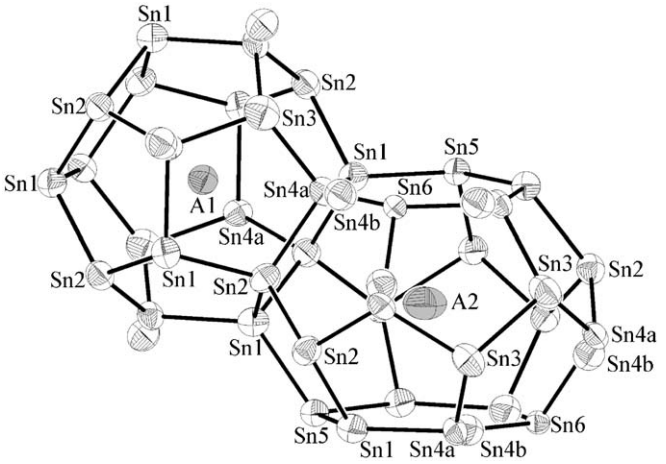

Fig. 2. Partial view of the $Rb_{1.42}Cs_{6.58}Sn_{44}$ (**2**) crystal structure. Displacement ellipsoids are drawn at the 90% probability level. Site occupation factors (SOF) for A1: SOF(Rb) = 0.46, SOF(Cs) = 0.54 and A2: SOF(Rb) = 0.08, SOF(Cs) = 0.92.

Table 2
Atomic coordinates and equivalent isotropic displacement parameters for **1**–**3**.

Atom	Site	*x*	*y*	*z*	SOF	$U_{eq}/Å^2$
$Rb_{2.12}Cs_{5.88}Sn_{44}$ (**1**)						
Rb/Cs1	16*a*	0.5	0.5	0	0.60(2)/0.40(2)	0.0210(8)
Rb/Cs2	48*g*	0.625	0.24837(4)	0.00163(4)	0.15(2)/0.85(2)	0.0406(5)
Sn1	96*h*	0.50086(3)	0.34658(3)	0.05590(3)	1	0.0215(2)
Sn2	96*h*	0.59429(3)	0.40942(3)	0.08968(3)	1	0.0201(2)
Sn3	32*e*	0.59124(3)	0.40876(3)	−0.09124(3)	1	0.0287(4)
Sn4a	96*h*	0.5030(1)	0.3484(2)	−0.0597(2)	0.333	0.0152(8)
Sn4b	96*h*	0.5009(1)	0.3271(1)	−0.0669(1)	0.667	0.0248(5)
Sn5	24*d*	0.5	0.25	0.125	1	0.0187(4)
Sn6	24*c*	0.5	0.25	−0.125	0.333	0.0111(8)
$Rb_{1.42}Cs_{6.58}Sn_{44}$ (**2a**)						
Rb/Cs1	16*a*	0.5	0.5	0	0.46(2)/0.54(2)	0.0239(7)
Rb/Cs2	48*g*	0.625	0.24833(3)	0.00167(3)	0.08(1)/0.92(1)	0.0449(5)
Sn1	96*h*	0.50089(3)	0.34666(3)	0.05595(3)	1	0.0240(2)
Sn2	96*h*	0.59436(3)	0.40945(3)	0.08967(3)	1	0.0233(2)
Sn3	32*e*	0.59127(3)	0.40873(3)	−0.09127(3)	1	0.0318(4)
Sn4a	96*h*	0.5028(2)	0.3484(1)	−0.0597(2)	0.333	0.0203(8)
Sn4b	96*h*	0.5011(1)	0.3272(1)	−0.0670(1)	0.667	0.0273(4)
Sn5	24*d*	0.5	0.25	0.125	1	0.0206(3)
Sn6	24*c*	0.5	0.25	−0.125	0.333	0.0156(7)
$Rb_{1.46}Cs_{6.54}Sn_{44}$ (**2b**)						
Rb/Cs1	2*a*	0	0	0	0.46(1)/0.54(1)	0.0235(4)
Rb/Cs2	6*d*	0.25	0.5	0	0.09(1)/0.91(1)	0.0478(3)
Sn1	6*c*	0.25	0	0.5	0.667	0.0175(2)
Sn2	16*i*	0.18299(2)	0.18299(2)	0.18299(2)	1	0.0252(1)
Sn3a	24*k*	0	0.30551(7)	0.1137(1)	0.667	0.0221(2)
Sn3b	24*k*	0	0.3443(1)	0.1338(2)	0.333	0.0260(4)
$Rb_{1.32}Cs_{6.68}Sn_{44}$ (**3**)						
Rb/Cs1	16*a*	0.5	0.5	0	0.40(2)/0.60(2)	0.0219(6)
Rb/Cs2	48*g*	0.625	0.24830(4)	0.00170(4)	0.08(1)/0.92(1)	0.0409(5)
Sn1	96*h*	0.50083(3)	0.34660(3)	0.05596(3)	1	0.0219(2)
Sn2	96*h*	0.59430(3)	0.40944(3)	0.08974(3)	1	0.0209(2)
Sn3	32*e*	0.59128(3)	0.40872(3)	−0.09128(3)	1	0.0296(3)
Sn4a	96*h*	0.5028(2)	0.3482(2)	−0.0598(2)	0.333	0.0153(7)
Sn4b	96*h*	0.5010(1)	0.3272(1)	−0.0670(1)	0.667	0.0253(4)
Sn5	24*d*	0.5	0.25	0.125	1	0.0189(3)
Sn6	24*c*	0.5	0.25	−0.125	0.333	0.0126(7)

in the center of the *tkad*. Furthermore, the unit cell expands to some extent as the Cs content of the clathrates increases.

Multi-temperature diffraction experiments were performed on the single-crystal with the composition $Rb_{1.42}Cs_{6.58}Sn_{44}$. Single crystals of superstructure reflections of $Rb_{1.42}Cs_{6.58}Sn_{44}$ disappeared at 373 K and the full data collection at this temperature resulted in the composition $Rb_{1.46}Cs_{6.54}Sn_{44}$ (**2b**) in the primitive space group $Pm\bar{3}n$ (Tables 1–3). This high-temperature modification resembles well the structure of β-A_8Sn_{44} (A = Rb, Cs) [5,6]. The subsequent data collection at room temperature showed that the cell transformed again to I-centred without alternation of the crystallinity or the ordering of the alkali metals in the framework cavities.

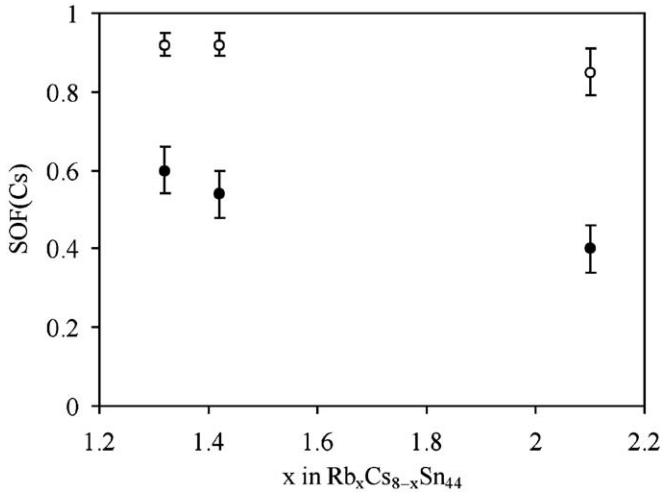

Fig. 3. Site occupation factors (SOF) of the Cs atoms with 3σ deviations in *pdod* (closed circles) and *tkad* (open circles) for the compounds **1**–**3**.

Some other cases of type-I clathrates with two different kinds of encaged atoms have been so far structurally characterized: (a) the compound $K_{1.6}Cs_{6.4}Sn_{44}$ [1] that also exhibits mixed occupancy in both cationic positions (b) solid solutions of polycationic $[Sn_{24}P_{19.3}]Br_xI_{8-x}$ ($0 \le x \le 8$) and $[Sn_{24}P_{19.3}]Cl_yI_{8-y}$ ($y \le 0.8$) [12] (c) $Na_2Ba_6Si_{46}$ with *pdod* and *tkad* fully occupied by Na and Ba, respectively [13] and (d) $Eu_2K_6Ga_{10}Ge_{36}$ [14] also with fully ordered cations. The rattling of the encaged cations is regarded as a significant (in)stability factor and therefore the well fitting Cs radius in the relatively large framework cavities of the Sn atoms justifies the trend towards type-I clathrate formation. Lighter alkali metals would lead to both type-I and type-IX (or *cP*124) $A_{8-x}Sn_{25}$ clathrates, whereas mixing of two alkali metals of very different size such as Na and Cs would give rise to type-II and type-III clathrates [15,16].

Fig. 4 depicts the temperature dependence of the electrical resistivity of **2** and Rb_8Sn_{44} (insert Fig. 4) for cooling and warming sequences. Both samples exhibit low electrical conductivities in agreement with the Zintl concept [3] which predicts empty conduction bands for **2** and Rb_8Sn_{44}. Down to 360 K, $\rho(T)$ increases with decreasing temperature. In the temperature

Table 3
Anisotropic displacement parameters for **1–3** (in Å^2).

Atom	U_{11}	U_{22}	U_{33}	U_{12}	U_{13}	U_{23}
$Rb_{2.12}Cs_{5.88}Sn_{44}$ (**1**)						
Rb/Cs1	0.0210(8)	U_{11}	U_{11}	0	0	0
Rb/Cs2	0.0256(7)	0.0482(7)	U_{22}	0	0	−0.0024(6)
Sn1	0.0192(4)	0.0211(4)	0.0243(4)	0	0.0009(3)	0
Sn2	0.0219(4)	0.0185(4)	0.0200(4)	0.0023(3)	−0.0039(3)	−0.0004(3)
Sn3	0.0287(4)	U_{11}	U_{11}	0.0062(3)	U_{12}	U_{12}
Sn4a	0.016(1)	0.016(2)	0.014(1)	0	−0.003(1)	0
Sn4b	0.0229(8)	0.026(1)	0.025(1)	0	0.0014(7)	0.004(1)
Sn5	0.0182(5)	U_{11}	0.0198(8)	0	0	0
Sn6	0.010(1)	U_{11}	0.013(2)	0.002(2)	0	0
$Rb_{1.42}Cs_{6.58}Sn_{44}$ (**2a**)						
Rb/Cs1	0.0239(7)	U_{11}	U_{11}	0	0	0
Rb/Cs2	0.0286(7)	0.0530(6)	U_{22}	0	0	−0.0032(5)
Sn1	0.0227(4)	0.0227(4)	0.0267(4)	0	0.0011(3)	0
Sn2	0.0247(4)	0.0215(4)	0.0236(4)	0.0022(3)	−0.0036(3)	0
Sn3	0.0318(4)	U_{11}	U_{11}	0.0059(3)	U_{12}	U_{12}
Sn4a	0.022(1)	0.021(2)	0.018(1)	0.003(2)	0.001(1)	−0.004(2)
Sn4b	0.0260(7)	0.028(1)	0.0278(9)	0.001(1)	0.0013(6)	0.0025(9)
Sn5	0.0198(4)	U_{11}	0.0222(7)	0	0	0
Sn6	0.015(1)	U_{11}	0.015(1)	0.001(1)	0	0
$Rb_{1.46}Cs_{6.54}Sn_{44}$ (**2b**)						
Rb/Cs1	0.0235(4)	U_{11}	U_{11}	0	0	0
Rb/Cs2	0.0281(5)	0.0576(4)	U_{22}	0	0	0
Sn1	0.0188(5)	0.0169(3)	0.0169(3)	0	0	0
Sn2	0.0252(1)	U_{11}	U_{11}	−0.0038(1)	U_{12}	U_{12}
Sn3a	0.0223(3)	0.0190(5)	0.0251(4)	0	0	−0.0029(3)
Sn3b	0.0240(7)	0.028(1)	0.0256(9)	0	0	0.0063(7)
$Rb_{1.32}Cs_{6.68}Sn_{44}$ (**3**)						
Rb/Cs1	0.0219(6)	U_{11}	U_{11}	0	0	0
Rb/Cs2	0.0258(6)	0.0484(6)	U_{22}	0	0	0
Sn1	0.0205(4)	0.0213(4)	0.0240(4)	0	0.0008(3)	0.0007(3)
Sn2	0.0229(4)	0.0190(4)	0.0207(4)	0.0024(3)	−0.0037(3)	0
Sn3	0.0296(3)	U_{11}	U_{11}	0.0059(3)	U_{12}	U_{12}
Sn4a	0.017(1)	0.016(2)	0.013(1)	0	0	0
Sn4b	0.0234(7)	0.026(1)	0.0263(9)	0	0.0009(6)	0.0029(9)
Sn5	0.0184(4)	U_{11}	0.0199(7)	0	0	0
Sn6	0.012(1)	U_{11}	0.014(2)	0.002(1)	0	0

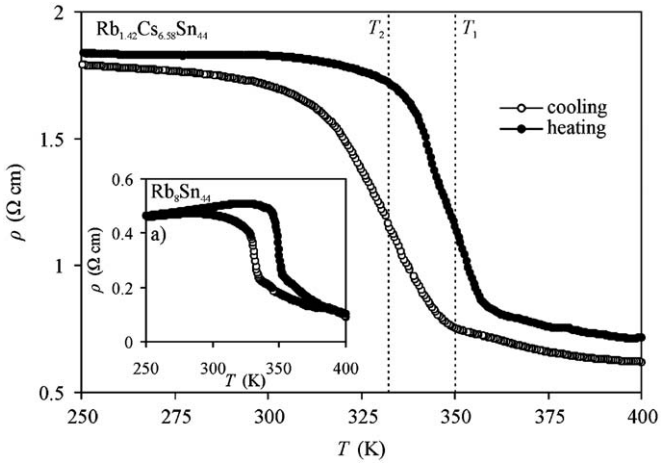

Fig. 4. Electrical resistivity of $Rb_{1.42}Cs_{6.58}Sn_{44}$ on a linear scale between 250 and 400 K. The dashed lines indicate the reversal points of the cooling-down and warming-up $\rho(T)$ sequences. Insert (a) shows the temperature dependence of Rb_8Sn_{44}.

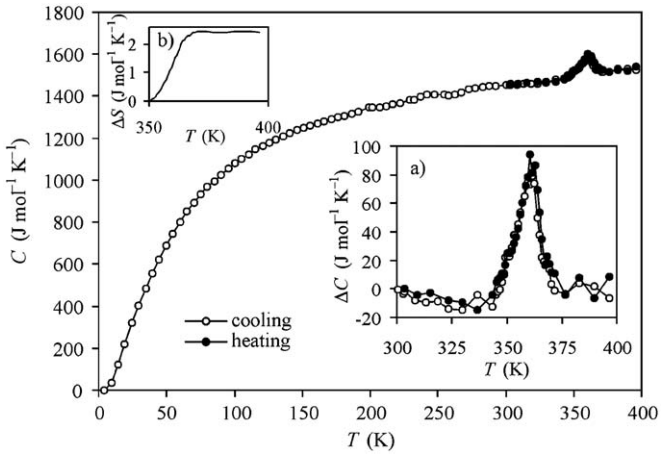

Fig. 5. Specific heat C as a function of temperature T for $Rb_{1.42}Cs_{6.58}Sn_{44}$. Insert (a) shows an enlarged view of the $C(T)$ anomaly after subtracting a linear background mainly due to phonon contributions. Insert (b) displays the entropy change, observed during the phase transition.

range 360–310 K, the resistivity increase is even more pronounced, and characterized by appreciable differences between cooling and heating sequences. Such reversible, hysteretical temperature dependence of the $\rho(T)$ data hints for a first-order phase transition [17]. For **2** the characteristic temperatures of the reversal points of the cooling ($T_2 \approx 332$ K) and heating ($T_1 \approx 350$ K) $\rho(T)$ sequences are marked by dashed lines in Fig. 4. In both Rb_8Sn_{44} and $Rb_{1.42}Cs_{6.58}Sn_{44}$ the $\rho(T)$ increases during the disorder–order by a factor of 4. This effect may be caused by the alternation of the concentration of vacancies in the domains of the crystal.

The temperature dependence of the specific heat of **2** is displayed in Fig. 5. In the temperature range 340–380 K, a pronounced symmetric anomaly with its maximum at 361 K is observed. The symmetric shape of the ($C(T)$) peak is indicative of a first-order phase transition. In contrast to the resistivity data based on a single-crystal study no hysteretical behavior between cooling and warming sequences (insert (a) in Fig. 5) was observed in case of the pressed powder sample employed in the $C(T)$ studies. Furthermore, the temperature range where the specific heat anomaly develops, occurs at slightly higher values

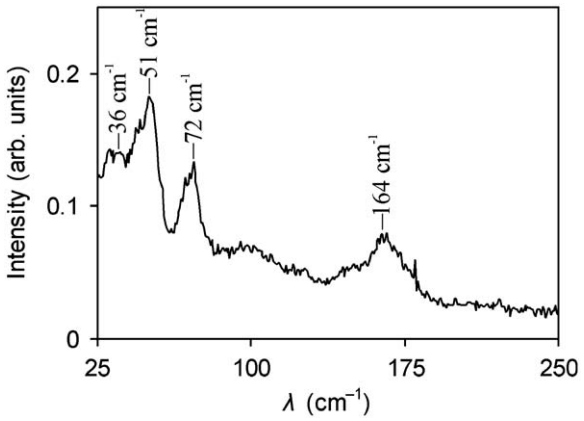

Fig. 6. Raman spectrum of $Rb_{1.42}Cs_{6.58}Sn_{44}$ at ambient temperature and pressure.

(~370–330 K) relative to the resistivity hysteresis curve between T_1 and T_2 (Fig. 4). Such unusual behavior has been also reported for the type-IX clathrate compound Ba_6Ge_{25}, where the main specific heat anomaly is also due to a structural first-order phase transition [17]. To have a closer look on the phase transition of **2**, the specific heat ΔC (insert (a) in Fig. 5) was obtained by subtracting a linear background mainly due to phonon contributions. The resulting structural entropy of the anomaly per mole $Rb_{1.42}Cs_{6.58}Sn_{44}$ (insert (b) in Fig. 5) is about 2.5 J mol^{-1} K^{-1}, which accords with a pronounced first-order structural phase transition.

The Raman spectrum of **2** at ambient temperature and pressure is depicted in Fig. 6 and resembles well that of Rb_8Sn_{44} and Cs_8Sn_{44} [18]. The bands at frequencies above 44 cm^{-1} are attributed to the Sn framework vibrations, whereas the vacancy-induced band is found around 70 cm^{-1}. Two broad bands at 31 and 36 cm^{-1} are attributed to guest rattling vibrations. By considering the general rule that there is no Raman active guest-atom vibration in the small *pdod* cage for type-I clathrates [10], these vibrational modes stem from the large *tkad* cages (SOF(Rb) = 0.08 and SOF(Cs) = 0.92). Since the Cs atoms is about 1.5 times heavier than the Rb atoms, their rattling frequencies are expected to be different from each other, i.e. Raman bands will be broad due to heavier Cs and lighter Rb motions [19].

4. Conclusion

Both types of framework cavities in $Rb_xCs_{8-x}Sn_{44}\square_2$ show clear trend towards encapsulation of the larger alkali metal, namely Cs rather than Rb. Nevertheless, a certain homogeneity range close to the composition $Rb_2Cs_6Sn_{44}$ is observed, as well as cationic disorder even for long-annealed samples. The electrical resistivity and specific heat measurements of **2** locate the structural order–disorder phase transition in the temperature range 333–373 K. The hysteresis displayed by the electrical resistivity data in combination with the symmetric shape of the specific heat anomaly suggests that the transformation is of first-order type and is characterized by an entropy change of about 2.5 J mol^{-1} K^{-1}. The more disordered modification of $Rb_{1.42}Cs_{6.58}Sn_{44}$ exhibits higher electrical flow than the ordered modification.

Acknowledgments

The authors wish to thank the European Union's RTN program (Eu-project Nr. HPRN-CT 2002-00193) for the financial support.

This work was also partially supported by a Grant-in-Aid for Scientific Research on Priority Areas (New Materials Science Using Regulated Nano Spaces—Strategy in Ubiquitous Elements, Grant no. 19051008) from the Ministry of Education, Culture, Sports, Science, and Technology of Japan.

Appendix A. Supplementary material

Supplementary data associated with this article can be found in the online version at doi:10.1016/j.jssc.2009.07.034.

References

[1] J.T. Zhao, J. Corbett, Inorg. Chem. 33 (1994) 5721–5726.
[2] H.-G. von Schnering, R. Kröner, M. Baitinger, K. Peters, R. Nesper, Yu. Grin, Z. Kristallogr. NCS 215 (2000) 205–206.
[3] C. Myles, J. Dong, O. Sankey, Phys. Rev. B 64 (2001) 165202(11).
[4] F. Dubois, T.F. Fässler, J. Am. Chem. Soc. 127 (2005) 3245–3264.
[5] A. Kaltzoglou, S.D. Hoffmann, T.F. Fässler, Eur. J. Inorg. Chem. (2007) 4162–4167.
[6] A. Kaltzoglou, T.F. Fässler, M. Christensen, S. Johnsen, B. Iversen, I. Presniakov, A. Sobolev, A. Shevelkov, J. Mater. Chem. 18 (2008) 5630–5637.
[7] T. Roisnel, J. Rodriguez-Carvajal, FULLPROF, version 3.20 LLB-LCSIM, March 2005.
[8] G.M. Sheldrick, Acta. Crystallogr. A 64 (2008) 112–122.
[9] T. Kume, H. Fukuoka, T. Koda, S. Sasaki, H. Shimizu, S. Yamanaka, Phys. Rev. Lett. 90 (2003) 155503.
[10] J.S. Tse, T. Iitaka, T. Kume, H. Shimizu, K. Parlinski, H. Fukuoka, S. Yamanaka, Phys. Rev. B 72 (2005) 155441.
[11] H. Shimizu, T. Iitaka, T. Fukushima, T. Kume, S. Sasaki, N. Sata, Y. Ohishi, H. Fukuoka, S. Yamanaka, J. Appl. Phys. 101 (2007) 063549.
[12] J. Zaikina, W. Schnelle, K. Kovnir, A. Olenev, Yu. Grin, A. Shevelkov, Solid State Sci. 9 (2007) 664–671.
[13] M. Baitinger, H.-G. von Schnering, J.-H. Chang, K. Peters, Yu. Grin, Z. Kristallogr. NCS 222 (2007) 87–88.
[14] S. Paschen, S. Budnyk, U. Köhler, Yu. Prots, K. Hiebl, F. Steglich, Yu. Grin, Physica B 383 (2006) 89–92.
[15] S. Bobev, S. Sevov, J. Am. Chem. Soc. 121 (1999) 3795–3796.
[16] S. Bobev, S. Sevov, J. Am. Chem. Soc. 123 (2001) 3389–3390.
[17] S. Paschen, V.H. Tran, M. Baenitz, W. Carrillo-Cabrera, Yu. Grin, F. Steglich, Phys. Rev. B 65 (2002) 134435.
[18] H. Shimizu, T. Imai, T. Kume, S. Sasaki, A. Kaltzoglou, T.F. Fässler, Chem. Phys. Lett. 464 (2008) 54–57.
[19] C.W. Myles, K. Biswas, E. Nenghabi, Physica B 401–402 (2007) 695–698.